Engineering Science and Technology, an International Journal 22 (2019) 956–965

HOSTED BY

Contents lists available at ScienceDirect

Engineering Science and Technology, an International Journal

journal homepage: www.elsevier.com/locate/jestch

Full Length Article

Optimization of rotary ultrasonic drilling of optical glass using Taguchi method and utility approach

Vikas Kumar *, Hari Singh

Department of Mechanical Engineering, National Institute of Technology, Kurukshetra 136119, India

ARTICLE INFO

Article history:
Received 7 October 2017
Revised 16 January 2019
Accepted 13 February 2019
Available online 21 February 2019

Keywords:
Abrasive
Ultrasonic drilling
Utility
ANOM
Taguchi

ABSTRACT

This work focuses on studying the impact of process parameters on the machining performance of rotary ultrasonic drilling of BK-7 glass and improving the machining efficacy by simultaneous optimization of conflicting output responses using utility approach. Taguchi based L9 array has been employed for framing the experimental work and to optimize output characteristics individually. Feed rate, tool rotational speed and ultrasonic power have been elected to understand their impact on material removal rate (MRR) and surface roughness (SR). Analysis of means (ANOM) has been implemented on raw data to identify the % contribution of statistically significant factors. Utility approach has been executed for simultaneous optimization of performance attributes. Middle level of feed along with highest levels of tool rotation speed and ultrasonic power, were predicted as optimal solution for superior performance. Feed was found to have maximum impact on MRR and SR followed by tool rotation speed and ultrasonic power. All the predicted results agreed well with experimental results at 95% confidence level. SEM micrographs of machined surfaces showed the presence of plastically deformed regions at lower levels of feed; whereas higher feed led to dominance of brittle fracture. Further, SEM micrographs revealed the occurrence of grain pullout, grain fracture and bond fracture of lateral as well as end face of the tool.

1. Introduction

The applications of optical glass BK7 are growing rapidly especially in optic and laser industry [1]. BK7 possesses superlative combination of high hardness, chemical inertness and high transmission with low thermal expansion co-efficient. Rotary ultrasonic machining (RUM) is being preferred in industries for machining of brittle materials and this has also attracted the attention of researchers. It has many variants like rotary ultrasonic grinding (RUG), rotary ultrasonic scratching (RUS), rotary ultrasonic milling (RUM), rotary ultrasonic texturing (RUT), and rotary ultrasonic drilling (RUD) etc. [2]. For the current investigation RUD has been used for machining of BK7 as drilling has paramount importance in manufacturing sector. Drilling accounts for approximately 40% of machining operations [3]. Drilling of advanced brittle materials is hard to accomplish with conventional machining processes. Limitations like low material removal rate (MRR), poor surface finish, excessive chipping, low aspect ratio, high tool wear and geometrical inaccuracies are being encountered during conventional machining processes. All these factors significantly affect the quality and precision of finished product. To cope up with highest quality standards, industries are looking for highly precise machining solutions. RUM has the potential to meet these expectations as it is capable of providing high MRR, superior finish, high aspect ratio, absence of heat affected zone with relatively low tool wear due to its superior material removal mechanism [4,5].

RUM is a direct contact advanced machining modus operandi that collaborates the capabilities of abrasive grinding and ultrasonic machining (USM). Neither of them achieves the material removal rate of RUM independently [6,7]. Under the combined effect of rotation, downward axial feed and ultrasonic vibrations, abrasive particles coated over tool follow the helical sinusoidal trajectory.

Gupta et al. inferred crack free RUD of bones with lower cutting forces and torque at higher levels of tool rotational speed and tool amplitude [8]. Fernando et al. inferred the effectiveness of cushioning effect of backing plate to control the delamination in RUD of carbon fiber reinforced polymer (CFRP) [9]. Gupta et al. observed increase in cutting temperature with increase in all the input variables except vibration amplitude during RUD of bones [10]. Jain et al. reported minimum edge chipping area at lower levels of

* Corresponding author.
E-mail addresses: vikas.thermal@gmail.com (V. Kumar), hsinghfme@nitkkr.ac.in (H. Singh).

Peer review under responsibility of Karabuk University.

https://doi.org/10.1016/j.jestch.2019.02.004
2215-0986/

vibration amplitude, feed rate and frequency while performing μ-RUD on borosilicate glass [11]. Wang et al. successfully curbed the edge chipping during RUD of brittle materials by using novel tools [12]. Wang et al. reported explicit dependency of edge chipping over cutting force during RUD of blind holes in quartz [13]. Huiting et al. observed significant reduction in cutting forces with increasing spindle speed at lower feed during RUD of SiCp/Al, which not only improved the hole accuracy but also suppressed chipping [14]. Ning et al. developed a mechanistic ultrasonic amplitude model based on the cutting forces produced during RUD of brittle material [15]. Feng et al. reported reduction in tearing at hole exit during RUD of C/SiC composite as a consequence of reduction in thrust force [16]. Cadorin et al. fabricated a 3D woven CFRP composite and drilled it with twist drill and electroplated core drill. Authors focused on studying the effect of machining variables (feed rate, spindle speed) and tool configuration on thrust force, surface roughness, delamination and wear mechanism. The core drills were observed to deliver superior performance than twist drill in enhancing the machining quality and reducing delamination [17]. Krishnaraj et al. drilled stacks made up of CFRP composite and aluminium to study the effect of process parameters such as feed rate, drill diameter and spindle speed on thrust force and torque. Further, analytical models developed for predicting output responses using artificial neural network were found to be more accurate than those developed using regression analysis. Feed and drill diameter had significant impact on output responses; whereas spindle speed had the minimum impact [18]. Prakash et al. compared performance of router tools with fluted twist drill for edge trimming of CFRP. Considering the complex tool profiles, acoustic emission signals were employed to measure the machining performance in terms of cutting force, surface roughness and delamination. Router tools with trapezoidal shape were reported to give superior surface finish that too without delamination due to substantial reduction in cutting forces as a consequence of formation of smaller discontinuous chips [19]. Fernando et al. used drilling variant of RUM on CFRP composites for studying the effect of abrasive variables namely abrasive size and concentration over output indices such as cutting force, torque and surface roughness. Cutting force was reported to upsurge with increase of abrasive concentration and size but didn't show any significant impact on surface roughness [20]. Wang et al. first time ever attempted to investigate the impact of tool orientation and other machining parameters–tool rotation speed, feed, depth of cut and vibration amplitude during edge trimming of CFRP. Edges trimmed with tool end face were reported to be of superior finish due to formation of smaller sized chips and micro-cracks. On the other hand, tool side face resulted in generation of lower cutting forces [21]. Song et al. processed the dental ceramics with and without ultrasonic vibration on a machining setup capable of rotating the cutting tool upto 200,000 RPM. Authors proposed the processing of dental ceramics using ultrasonic energy for improving their lifetime as a consequence of reduced cutting forces within the range of 40–50%. Such large reduction in cutting forces significantly minimized the chipping damage as well as surface flaws even though the fracture mode remained brittle [22]. Jain et al. emphasized on studying the tool wear pattern under the effect of various machining variables while drilling micro holes in micro glass valve with RUM. Regression model was developed for tool wear in terms of tool RPM, distance moved per stroke, feed, vibration amplitude and frequency. Tool wear was found to vary in direct proportion to tool RPM and inverse proportion to depth of cut. Tool wear didn't follow any specific trends with feed, amplitude and frequency [23]. Wang et al. formulated a cutting force model to examine the effect of cutting force on ultrasonic amplitude during RUD of brittle materials. The developed model yielded the critical value of cutting force beyond which there would be sudden increase in cutting force leading to poor RUD efficiency. Experimental data from RUD on quartz, sapphire and C/SiC verified the prediction accuracy of developed model [24]. Fernando et al. performed RUD on CFRP and used OFAT approach to see the impact of changing the tool configuration on the performance. Configuration of tool was changed by varying the end face angle termed as positive, negative and zero angle. Tool end face angle was reported to have more influence over delamination comparative to cutting force and tool with positive end angle yielded the best performance [25].

Literature highlighted that researchers have overlooked the process optimization of rotary ultrasonic drilling and one factor at a time (OFAT) approach preferred by them lacks in concurrent optimization of multiple responses. This gap can be filled by implementing design of experiments (DOE) statistical tools like Taguchi Methods coupled with utility for multi-response optimization. In past, researchers performed the experimental work in narrow range of ultrasonic power (30–50%). So, ultrasonic power range was broadened (30–70%) to throw more light on the uncharted side of RUD.

This paper concentrates on the performance analysis of Rotary Ultrasonic Drilling of BK7 in terms of output responses (Material removal rate, Surface roughness) under the combined influence of input variables (ultrasonic power, tool rotational speed and feed rate). Taguchi based L9 array has been used to frame the experimental work and for optimization of individual response. Thereafter, utility has been executed for simultaneous optimization of output responses [26–30]. The output of this research work would add to the knowledge domain and database of machining of BK7 glass.

2. Experimental set-up and data collection

The BK7 glass was selected as the work-piece material. The size of the work-piece is 50 mm × 50 mm × 5 mm. Mechanical properties of BK7 have been indexed in Table 1.

Rotary ultrasonic machine (knee series 10, sonic mill, installed at NIT Kurukshetra, India) was used to perform the experimental work with a power rating of 1000 W. The ultrasonic power is used to control the amplitude of ultrasonic vibrations. According to manufacturer, ultrasonic power is directly proportional to the ultrasonic amplitude and there is direct correlation between these two. Machine is designed to attain maximum amplitude of 80 μm at its full power rating. The basic parts of RUM include the ultrasonic spindle, ultrasonic transducer, tool holder, power supply, coolant pump, filter and control panel to regulate the input variables. A detailed illustration of machining setup and enlarged view of machining zone are shown in Figs. 1 and 2 respectively.

Nomenclature of drill used for experimentation has also been depicted in Fig. 2 with specifications logged in Table 2. Blasocut BC 20 SW water emulsified cutting solution diluted with deionized water with 1:18 ratio (Blaster Swisslube Inc., NY, USA) flows through the hollow tool and coolant hose to take away the microchips/debris. Besides this, coolant also serves the purpose of faster heat transfer from the machining zone preventing heat affected zone (HAZ) formation and minimizing the friction effects to endorse the better machining ambience. The coolant pressure was kept constant at 30 lb per square inch (206.8 kPa).

One factor at a time approach (OFAT) was accomplished for pilot experiments ahead of main experimentation with the intent of selecting the feasible range of input variables and to foresee the impact of their variation over the output parameters. It also helped to exclude insignificant factor 'coolant pressure' from the main experimentation.

In the current work, three variables – feed rate (FR), tool rotational speed (TRS), and ultrasonic power (UP) – have been chosen

Table 1
Mechanical properties of BK7 glass.

Material	Density (g/cm^3)	Poisson's ratio	Vickers Hardness (N/mm^2)	Fracture Toughness (N/mm$^{3/2}$)	Young's Modulus (N/mm^2)
BK7 Glass	2.51	0.204	7.7×10^3	0.82	82×10^3

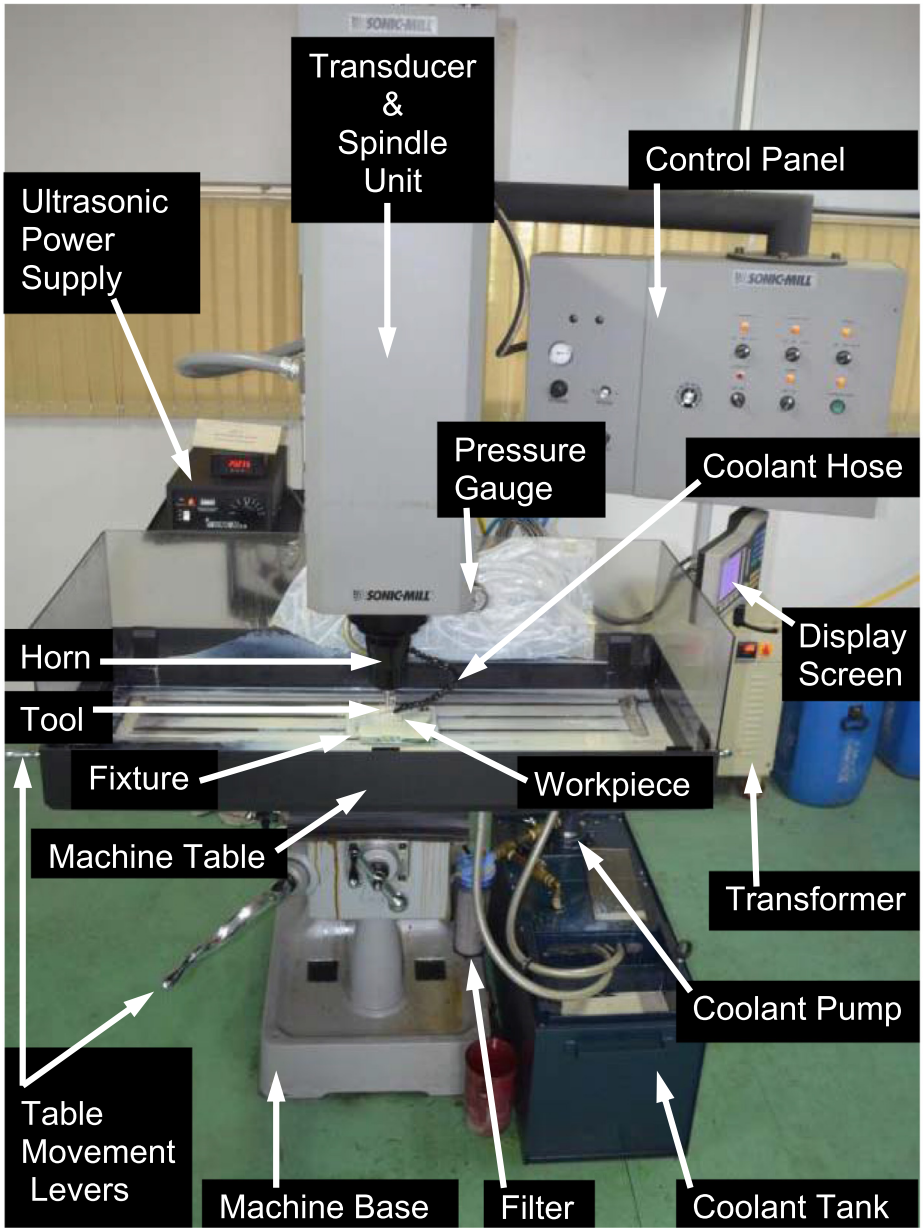

Fig. 1. Experimental set-up of rotary ultrasonic drilling (RUD).

after observing their remarkable influence on MRR and surface roughness (SR) during the pilot work. Input parameters with considered levels are given in Table 3. The orthogonal array L9 presented in Table 4 was generated by Minitab software (Version 17). Three input factors each with three levels lead to 9 experiments. Raw data as well as mean values of MRR and SR, has been tabulated in Table 5.

MRR and SR are the most common quantitative and qualitative responses respectively related to the drilled hole. MRR was calculated by the commonly used formula given in Eq. (1) [31–34]. Theoretical value of MRR in Eq. (1) is dependent greatly on the feed rate due to direct correlation with time. But practical MRR differs due to inclusion of high frequency ultrasonic vibrations as well as varying power (vibration amplitude). Insufficient resistance to oppose the high impact of ultrasonic energy by undrilled thickness in the end of drilling, results into instant removal of material. As a consequence of above mentioned conditions machining time varies.

$$MRR = \frac{\pi \times \left(D_h^2 - D_r^2\right) \times T}{4 \times t} \quad (1)$$

where

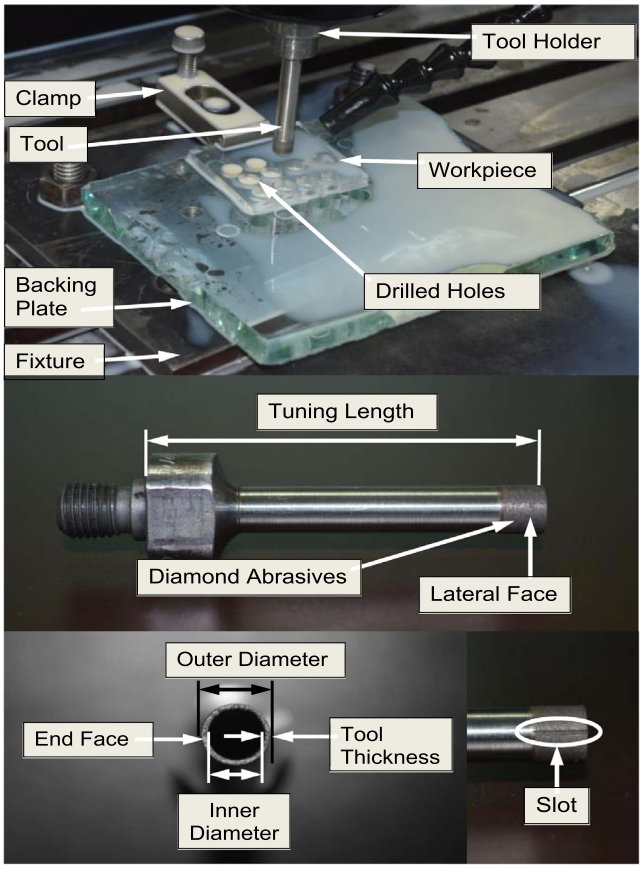

Fig. 2. Enlarged view of machining zone and tool nomenclature.

D_h: drilled hole diameter;
D_r: machined rod diameter
T: thickness of the work-piece;
t: time to drill the hole.

Surface roughness apparatus (Surfcom Flex 50A, Zeiss) has been used to compute the surface roughness.

3. Results and discussion

3.1. Single response optimization (SRO)

Single response optimization has been executed using Taguchi to tackle the situation when only one response is given the full preference over another to meet either qualitative or quantitative aspect of demand. Taguchi starts from performing analysis of means (ANOM) over raw data of output responses. ANOM Figures out the significant factors with their % contribution on output response. For a factor to be significant, it must have p-value less than 0.05 at 95% confidence level. Division of sum of squares (SS) of individual variables by the total sum of squares gives their relative % contribution on response of interest [35]. Then main effects plots are drawn to find the optimal parametric setting to predict the mean values of output responses.

3.1.1. Optimization of SR

In light of above statistical facts, ANOM data reported in Table 6, confirms that all the input variables – feed rate, tool rotational speed and ultrasonic power – have a significant impact on the SR. Being of smaller the better nature, $TRS_3FR_1UP_3$ (i.e. TRS = 5000 RPM, FR = 0.30 mm/min and UP = 70%) comes out as the optimal setting for SR as shown in Fig. 3 by small circles. Eq. (2) is used to find the predicted value of SR by using the mean values of output characteristic at the optimal parametric setting.

$$R_P = R_m + \sum_{i=1}^{q} \left(\bar{R}_i - R_m\right) \tag{2}$$

where

R_P = is predicted value of output response
R_m = mean value of response
$\bar{R}_i$ = mean value of response corresponding to optimal levels of variables
q = number of significant input variables

Replacing R with SR (response being optimized and predicted) the Eq. (2) can be rewritten as:

$$SR_P = \bar{SR}_m + \left(\bar{SR}_1 - \bar{SR}_m\right) + \left(\bar{SR}_2 - \bar{SR}_m\right) + \left(\bar{SR}_3 - \bar{SR}_m\right)$$

Or

$$SR_P = \bar{SR}_1 + \bar{SR}_2 + \bar{SR}_3 - 2\bar{SR}_m \tag{3}$$

whereSR_P = predicted surface roughness

$\bar{SR}_1$, $\bar{SR}_2$, $\bar{SR}_3$ are mean values of SR at the optimal level of first, second and third variable respectively as shown in Fig. 3.

$\bar{SR}_m = \bar{SR}_{MEAN}$ = mean value of SR as tabulated in Table 5

$\bar{SR}_1$ was calculated by taking the average of SR values corresponding to optimal level of first variable (i.e. TRS = 5000 RPM). Calculation illustration of $\bar{SR}_1$ is given below:

$$\bar{SR}_1 = \frac{0.293 + 0.549 + 0.662}{3} = 0.501$$

Similarly, $\bar{SR}_2 = 0.482$; $\bar{SR}_3 = 0.542$, using these values in Eq. (3), SR_P would be:

$$SR_P = 0.501 + 0.482 + 0.542 - 2(0.622)$$

$$SR_p = 0.281 \ \mu m$$

To check the reliability of predicted SR_P, Confidence Interval (C. I.) is also determined using Eq. (4) and ANOM data from Table 6.

$$C.I. = \sqrt{F_\alpha(n_1, n_2) V_e \left[\frac{1}{n_{eff}} + \frac{1}{R}\right]} \tag{4}$$

where

F_α (1, f_e) is *F* ratio at α% level of significance;
n_1 is always 1.
$n_1 = f_e$ = degrees of freedom (DOF) co-related to error in ANOM table (2 in present study)
V_e error variance or mean of squares for error

Table 2
Tool Specifications.

Outer diameter	Inner diameter	Tuning length	Abrasive material	Crimping rate	Abrasive size	Abrasive Concentration	Binder	Slots	Fabrication
8 mm	6.5 mm	57.30 mm	Diamond	25% by volume	220 mesh	100%	Metal	2	Sintering

Table 3
Investigated factors and their levels.

Sr. No	Process Variables	Designation	Variables level		
			−1	0	1
1.	Tool Rotational Speed (RPM)	TRS	3000	4000	5000
2.	Feed Rate (mm/min)	FR	0.30	0.60	0.90
3.	Ultrasonic Power (%)	UP	40	55	70

Table 4
L9 orthogonal array.

	In actual form			In coded form		
Trial number	TRS (RPM)	FR (mm/min)	UP (%)	TRS (RPM)	FR (mm/min)	UP (%)
1	3000	0.3	40	−1	−1	−1
2	3000	0.6	55	−1	0	0
3	3000	0.9	70	−1	1	1
4	4000	0.3	55	0	−1	0
5	4000	0.6	70	0	0	1
6	4000	0.9	40	0	1	−1
7	5000	0.3	70	1	−1	1
8	5000	0.6	40	1	0	−1
9	5000	0.9	55	1	1	0

Table 5
MRR and SR observations.

Raw data for responses							Mean values	
Exp. No.	MRR_1	MRR_2	MRR_3	SR_1	SR_2	SR_3	MRR_{MEAN} (mm^3/s)	SR_{MEAN} (μm)
1	0.0868	0.0834	0.0812	0.737	0.703	0.693	0.0838	0.711
2	0.2207	0.2198	0.2048	0.773	0.751	0.72	0.2151	0.748
3	0.3368	0.3269	0.3107	0.898	0.801	0.788	0.3248	0.829
4	0.1305	0.1292	0.1198	0.465	0.441	0.423	0.1265	0.443
5	0.2668	0.2641	0.2482	0.542	0.519	0.451	0.2597	0.504
6	0.2909	0.2811	0.2791	0.912	0.843	0.828	0.2837	0.861
7	0.1809	0.1784	0.175	0.307	0.298	0.274	0.1781	0.293
8	0.2567	0.2515	0.2511	0.577	0.543	0.527	0.2531	0.549
9	0.3643	0.3611	0.3555	0.685	0.659	0.642	0.3603	0.662
							$\bar{MRR}_m$ = 0.2317	$\bar{SR}_m$ = 0.622

Table 6
ANOM for SR.

Source	Degrees of freedom	Sum of Squares	Mean Squares	Fisher Ratio	p-value	% contribution
TRS	2	0.104164	0.052082	90.82	0.011	36.56
FR	2	0.138660	0.069330	120.90	0.008	48.67
UP	2	0.040931	0.020465	35.69	0.027	14.37
Error	2	0.001147	0.000537			0.40
Total	8	0.284902				
R^2 99.60%		R^2 adjusted 98.39%		R^2 predicted 91.85%		

R = number of confirmation experiments (3 for the current study)
n_{eff} = total number of effective tests

$$n_{eff} = \frac{total\ number\ of\ observations}{1 + sum\ of\ DOF\ associated\ with\ significant\ factors}$$

$$n_{eff} = \frac{9}{1 + DOF_{TRS} + DOF_{FR} + DOF_{UP}} = \frac{9}{1+2+2+2} = \frac{9}{7}$$

F_α (1, f_e) = 18.5 (Tabulated value at 95% confidence interval) [44]

$$V_e = .000537$$

$$C.I. = \pm 0.105$$

After calculating the confidence interval, experimental range of SR (S_{exp}) is calculated by using the Eq. (5).

$$SR_p - \text{C.I} \leqslant SR_{\exp} \leqslant SR_p + \text{C.I} \quad (5)$$

$$\text{or } 0.281 - \text{C.I} \leqslant SR_{\exp} \leqslant 0.281 + \text{C.I}$$

$$0.176 \leq SR_{exp} \leq 0.386 \quad (6)$$

Experimental value of SR 0.293 μm given in Table 9 at the optimal setting, satisfies the Eq. (6) and affirms the reliability of confidence interval.

3.1.2. Effect of variables on SR

Mean effects plot shown in Fig. 3 reveals the variation trend of SR with input variables. SR increases sharply with small increase in feed rate. Cutting forces increase with increase in feed rate [12,36]. The elevation in cutting forces leads to the deeper penetration depth of abrasives (coated on the lateral side of the drill) into the work piece [37]. Also, there is the possibility of embedding of debris into the work surface due to large cutting force. All these factors under the influence of ultrasonic hammering and larger cutting

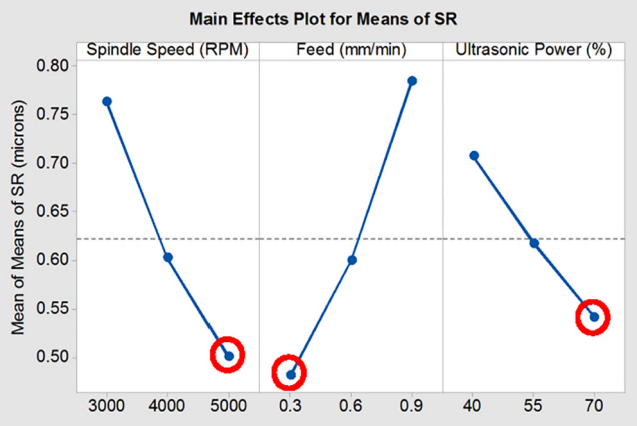

Fig. 3. Main effects plot for SR.

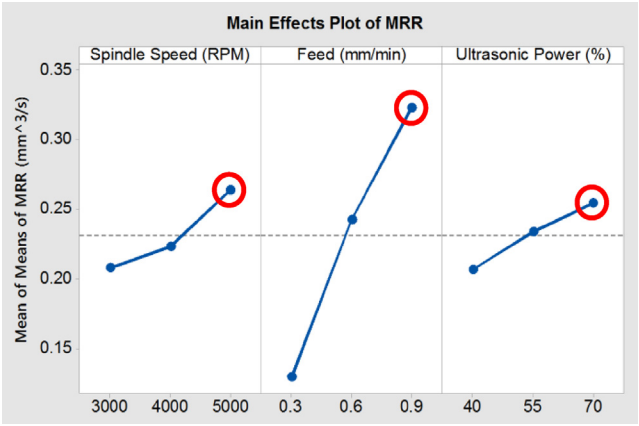

Fig. 4. Main effects plot for MRR.

force result into generation of local stresses. When these stresses exceed the material fracture limit, brittle fracture takes place due to the formation of big local grooves under the cutting point of abrasive. So, the sliding and rolling contact conditions generate poor surface quality at higher feed rates. After feed, tool rotational speed played a vital role to influence the SR. Surface quality started to improve with increase in RPM. The observed trends are in line with those reported by Cong and Ning [32,38]. This might be due to the probability of more frequent interactions between the abrasives and work-piece in a certain interval of time at higher spindle speed [32]. Rising ultrasonic power was found to improve surface quality. This could be due to the superior grinding action between the drill lateral surface and workpiece. The quality of grinding is promoted by the elevation in ultrasonic amplitude with an increase in power [39,40].

3.1.3. Optimization of MRR

ANOM data in Table 7 concludes that all the input variables significantly influence the MRR. By adopting the similar approach as that for SR, predicted value of material removal rate (MRR_P) has been calculated by using the optimal parametric condition TRS_3-FR_3UP_3 (i.e. TRS = 5000 RPM, FR = 0.90 mm/min and UP = 70%). Optimal condition has been shown in Fig. 4 by small circles. So, predicted value of MRR is

$MRR_P = 0.2638 + 0.3229 + 0.2542 - 2(0.2317)$

$MRR_P = 0.3775\ mm^3/s$

And

C.I. = ± 0.0411

And

$$0.3364 \leqslant MRR_{exp} \leqslant 0.4186 \quad (7)$$

The experimental value of MRR 0.3729 mm^3/s given in Table 9 at the optimal setting satisfies the Eq. (7) and affirms the reliability of confidence interval.

3.1.4. Effects of variables on MRR

Main effects plot among input parameters and MRR is shown in Fig. 4. MRR increases sharply with small upsurge in the feed rate due to increasing tool travel speed.

Power increment also enhanced the MRR. The increase in power has been reported to increase the amplitude of vibration [39], which has a direct impact on MRR [41]. The increased amplitude enhances the indentation depth of diamond abrasive resulting in more material removal. MRR will also increase with an increase in tool rotational speed. The increase in spindle speed increases MRR because indentation with increasing RPM gets deeper as a consequence of enhanced indentation forces [42]. Also, distance travelled by an abrasive when in contact with the work-piece, increases significantly as the spindle speed approaches the higher levels [37]. Combined effect of these phenomena gives rise to high MRR at higher RPM.

3.2. Multi response optimization using utility

In the forgoing investigation MRR and SR showed opposite changes with feed. So it becomes tough to achieve supreme value of one response without having negative impact on other parameter. Although Taguchi approach conveniently optimizes the individual responses but lacks in their concurrent optimization.

The utility concept is used to tackle such problems that have the capability of optimizing several aspects concurrently. Utility concept has already proved its usefulness by optimizing the performance of various machining processes [26,27,29,43]. Utility represents the usefulness of a product or service. The overall utility represents the sum of utility of all the individual parameters being considered. Overall utility is expressed as:

$$U(R_1, R_2, R_3 \cdots\cdots\cdots R_n) = \sum_{i=1}^{n} U_i(R_i) \quad (8)$$

where

Table 7
ANOM for MRR.

Source	Degrees of freedom	Sum of Squares	Mean Squares	Fisher ratio	p-value	% contribution
TRS	2	0.005009	0.002504	30.45	0.032	7.68
FR	2	0.056684	0.028342	344.65	0.003	86.88
UP	2	0.003384	0.001692	20.58	0.046	5.19
Error	2	0.000164	0.000082			0.25
Total	8	0.065241				
R^2 99.75%		R^2 adjusted 98.99%		R^2 predicted 94.90%		

R_i: measurement of response impact on product quality or performance
n: number of responses to decide the overall quality of product
U_i (R_i): utility of $\mathbf{i^{th}}$ response.

The Eq. number (8) can be modified as Eq. (9) to take care of the situation when different weightage is to be assigned to responses as per the requirement. The weight must be assigned in such a manner that their summation is equal to 1.

$$U(R_1, R_2, R_3 \cdots\cdots\cdots R_n) = \sum_{i=1}^{n} w_i U_i(R_i) \tag{9}$$

Utility concept starts with the formulation of preference scale whose value varies from 0 to 9. The preference scale is formed in such a manner that most acceptable values of a characteristic have utility around 9 and least acceptable values have utility around zero. The value of preference scale can be calculated by Eq. (10).

$$P_R = A \log\left\{\frac{R_n}{R_n^{\alpha}}\right\} \tag{10}$$

where R_n represents the experimental observation of R^{th} response for
n^{th} experimental setting; R_n^{α} is the just acceptable value of response (i.e. minimum value of response to be maximized and maximum value of response to be minimized)
A is constant which can be calculated by using Eq. (11).

$$A = \frac{9}{\log\left\{\frac{R_{opt}}{R_n^{\alpha}}\right\}} \tag{11}$$

where R_{opt} is the optimum predicted value of corresponding response.
Using Eq. (11), optimum predicted value of MRR 0.3775 mm^3/s and just acceptable value 0.0812 (from Table 5), the value of A for MRR (A_{MRR}) can be calculated as follow

$$A_{MRR} = \frac{9}{\log\left[\frac{0.3775}{0.0810}\right]} = 13.485$$

Similarly for optimum predicted value of SR 0.281 μm and just acceptable value 0.912 μm (maximum value of SR) the value of A for SR (A_{SR}) becomes:

$$A_{SR} = \frac{9}{\log\left[\frac{0.281}{0.898}\right]} = -17.837$$

By putting values of A_{MRR} and A_{SR} in Eq. (10) and denoting 'R' by MRR and SR respectively, preference scale Eqs. for MRR and SR can be written as follow

$$P_{MRR} = 13.485 \log\frac{MRR_n}{MRR_n^{\alpha}} = 13.485 \log\frac{MRR_n}{0.0812}$$

$$P_{SR} = -17.837 \log\frac{SR_n}{0.898}$$

where, MRR_n and SR_n represents the experimental observations of MRR and SR respectively for n^{th} experiment.
After assigning equal weightage of 0.5 to both the responses, utility values were calculated using Eq. (12). Then their mean values were computed which has been reported in Table 8.

$$U = w_{MRR} P_{MRR} + w_{SR} P_{SR} \tag{12}$$

Then main effects plot as shown in Fig. 5, was drawn considering the mean utility values to predict the optimal setting. Being of higher the better nature of utility, $TRS_3FR_2UP_3$ (i.e. TRS = 5000 RPM, FR = 0.60 mm/min and UP = 70%) emerges as the optimal setting for concurrent optimization of output responses as given in Table 9. Optimal setting has been depicted in Fig. 5 by small circles.

4. Microstructural analysis of machined surface and tool wear

The quality of machined holes has been shown in Fig. 6. The upper part is showing the hole entry side whereas lower part is showing the exit side of holes. Despite the use of backing material beneath the workpiece there was chipping at the exit side. Very little chipping damage was observed at the entry side. By this token, it can be concluded that at the starting of drilling, workpiece thickness was sufficient to counteract the cutting forces. But with the advancement of tool in workpiece surface workpiece thickness goes on decreasing and a stage comes when last few layers are not able to sustain the cutting forces and break suddenly that is termed as chipping. The chipping is still a key barrier in RUM and extensive research work is being done to curb it or eliminate it.

Machine surfaces were detected for all the experimental settings. For higher feed and low RPM, brittle fracture was the mode of material removal. While for lower feed and higher RPM, plastically deformed regions were also noticed which indicates that complex interaction between the abrasives and workpiece lead to a situation where depth of cut was less than critical depth of cut [45]. Consequently, material was removed due to ductile fracture along with brittle fracture. For clear illustration of different modes of material removal in RUM, SEM images of experiment 3, 7 and 1 have been shown. The machined surface corresponding to experiment 3 has been shown in Fig. 7 that shows the impact of highest level of feed (0.90 mm/min). Along with the brittle fracture of machined surface, some cracks were also detected. During the machining, a crack system develops underneath the tool tip. This crack system is composed of lateral, median and radial cracks. Lateral cracks travel parallel to machined surface and median cracks in perpendicular direction. Radial cracks travel at any other angles other than that of 0 and 90 degrees. The size of craters formed on machined surface due to abrasive depends on the extent of propagation of these cracks in material. Deeper and larger cracks remove bigger chunks of material resulting in severe brittle fracture.

The machined surface corresponding to experiment 7 has been shown in Fig. 8 that shows the impact of lowest level of feed (0.30 mm/min). Along with the brittle fracture of machined surface, some plastically deformed areas were also detected. These regions improved the surface quality of machined surfaces.

Further, Fig. 9 shows the machined surface corresponding to experiment number 1 with low feed rate of 0.30 mm/min. The machined surface was magnified to 10,000X for better view of plastically deformed regions. Other than these regions, Subsurface damage (SSD) was also visible beneath them. Usually subsurface damage is detected after polishing them. However, in current investigation, SSD was visible as the surfaces were naturally polished due to formation of plastically deformed regions.

Tool wear is an inevitable phenomenon in advance machining processes. Therefore, it becomes necessary to study the tool wear as it significantly affects the machining performance and economics. After completion of experimentation, lateral as well as end faces of tool were analyzed with scanning electron microscope (EVO 18, Germany). Three different kinds of tool wear mainly attritious wear, grain fracture and grain pullout (bond fracture) were noticed on both the surfaces as shown in Figs. 10 and 11. These types of wear have also been reported by other researchers for different abrasive machining processes [46].

In case of attritious wear, abrasive grains are worn due to erosion and their protrusion from mean tool profile reduces continu-

Table 8
Utility data based on output responses.

Exp. No.	Utility values			U_{mean}
	$U_1 = 0.5(MRR_1 + SR_1)$	$U_2 = 0.5(MRR_2 + SR_2)$	$U_3 = 0.5(MRR_3 + SR_3)$	
1	1.010	1.073	1.050	1.044
2	3.560	3.658	3.612	3.610
3	4.225	4.574	4.488	4.429
4	3.964	4.137	4.075	4.059
5	5.472	5.608	5.963	5.681
6	3.737	3.937	3.985	3.886
7	6.507	6.580	6.845	6.644
8	5.120	5.292	5.402	5.272
9	5.489	5.612	5.666	5.589

Table 9
Comparison of results.

Optimization Method	Response	Optimal setting	Predicted Value	Confirmatory Value
Single response optimization (Taguchi)	MRR	$TRS_3FR_3UP_3$	0.3775 mm^3/s	0.3729 mm^3/s
	SR	$TRS_3FR_1UP_3$	0.281 μm	0.293 μm
Multi response optimization (Utility)	MRR	$TRS_3FR_2UP_3$	–	0.2871 mm^3/s
	SR			0.471 μm

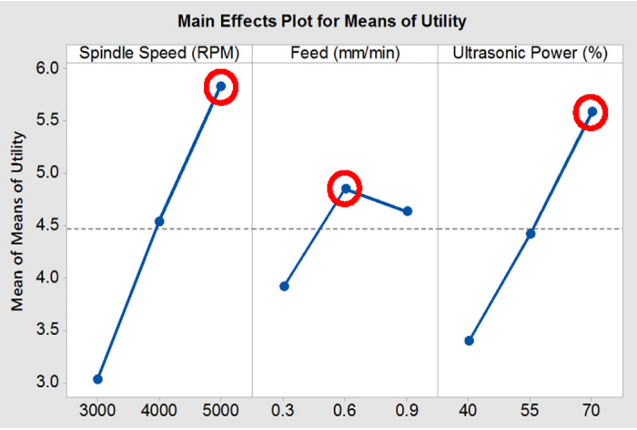

Fig. 5. Main effects plot for utility.

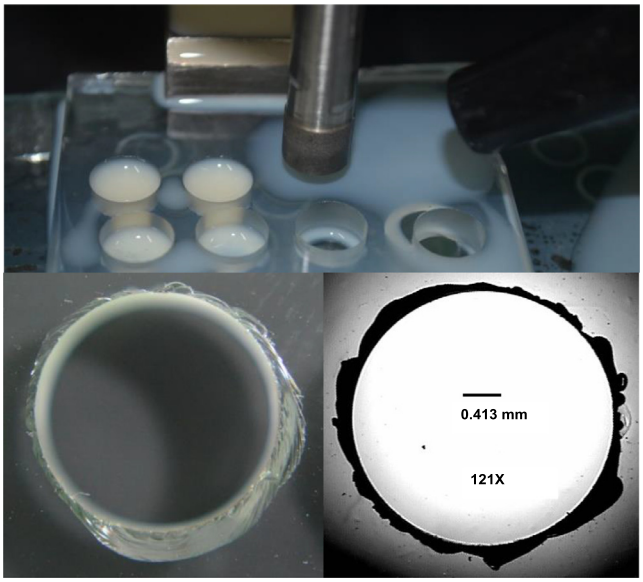

Fig. 6. Quality of drilled holes.

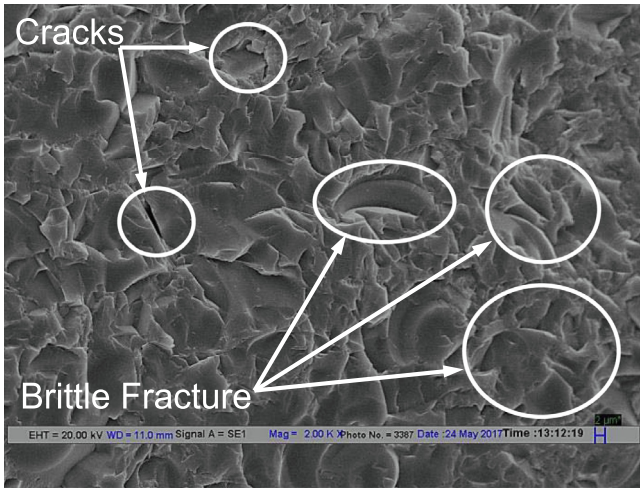

Fig. 7. SEM micrograph for exp. 3.

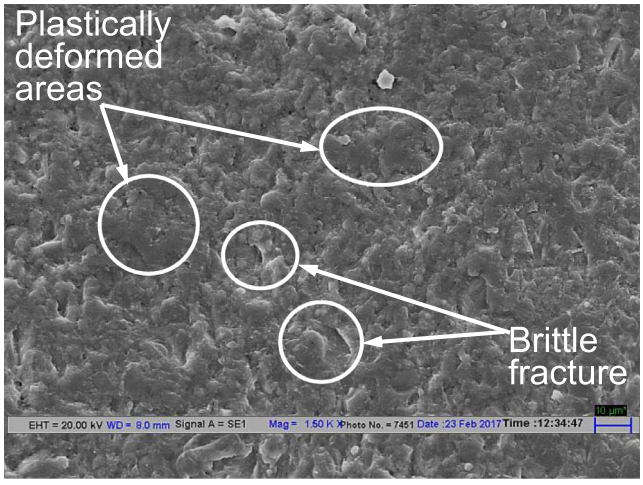

Fig. 8. SEM micrograph for exp. 7.

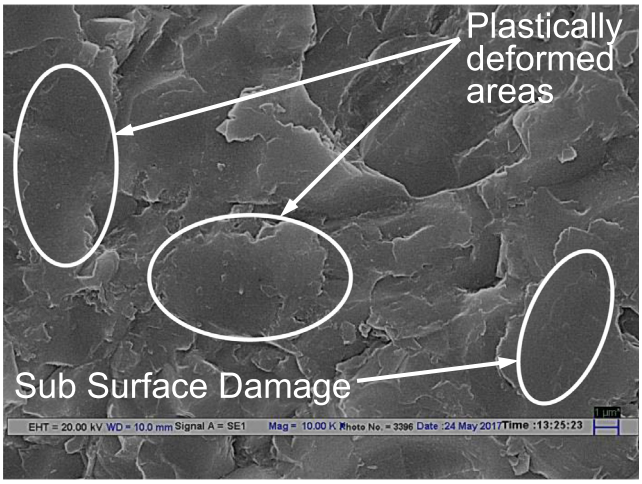

Fig. 9. SEM micrograph for exp. 1.

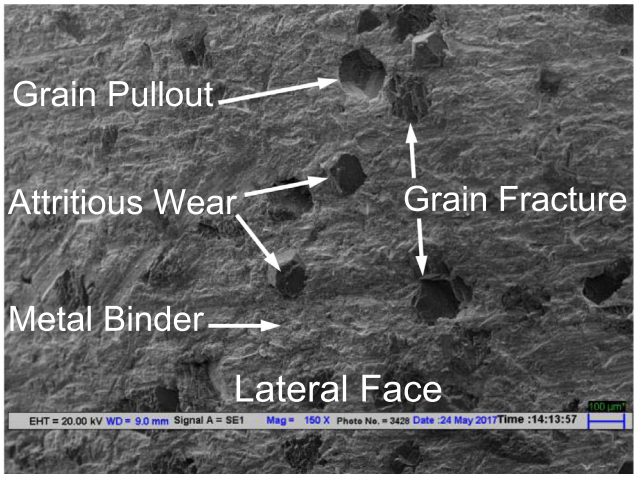

Fig. 10. SEM micrograph of tool lateral face.

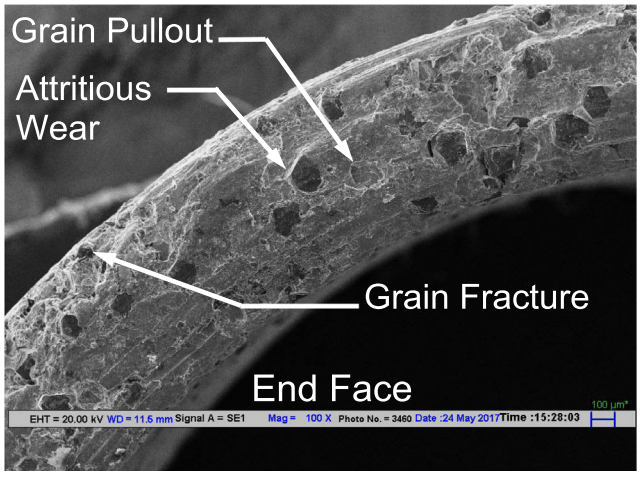

Fig. 11. SEM micrograph of tool end face.

ously. Consequently, abrasives become flat and lose their cutting effectiveness. On the other hand, in grain fracture, fragments of abrasive are removed due to brittle fracture within the abrasive itself. This partial fracture of abrasive grain gives rise to fresh cutting edges and retains the cutting effectiveness. Out of all the above-mentioned wear, grain pullout is the most severe as it results in complete dislodgement of abrasives from metal binder. It happens due to deformation of metal binder during machining that weakens the binding strength of binder around the abrasive. Because of it abrasives are completely removed from soft binding material. Not only grain pullout results into loss of active abrasive particles but also have negative effect on the form of cutting tool especially on the lateral face [46]. In case of sintered tools that have multi layers of abrasives, grain pullout possesses one advantage also; it leads to self-dressing of tool as the bottom layers come into play when upper adjacent layer is worn out.

5. Confirmation experiments

To check the reliability and accuracy of predictions made by Taguchi and utility approaches, confirmation experiments were performed at the predicted optimal settings. Predicted parametric setting for SR matched with one of the experimental settings, so predicted value was directly compared with this value. Three experiments were performed at the predicted optimal settings for MRR as well as concurrent optimization of both the responses. Then average of experimental values was taken. Final mean values along with corresponding optimal settings have been tabulated in Table 9. Low variation, observed between predicted and actual values validated the accuracy and reliability of experimental observations corresponding to optimal setting.

6. Conclusions

The work was carried out to identifying the significant factors to measure the performance of RUD in terms of MRR and SR. Utility approach has been executed for concurrent optimization of responses. The following conclusions have been drawn from this study:

1. All the investigated input variables have been found to be statistically significant for MRR and SR.
2. Feed was found to have contribution of 86.88% and 48.67% on MRR and SR respectively. Such high values show that feed must be chosen carefully to get better machining performance.
3. The optimized values of MRR and SR achieved with single response optimization have been found as 0.3729 mm^3/s and 0.293 μm respectively.
4. Multi-response optimization of MRR and SR yielded parametric setting of $TRS_3FR_2UP_3$ which has been validated through confirmation trials.
5. Material removal occurred due to brittle fracture as well as ductile fracture. SEM analysis of machined surfaces also showed presence of cracks and subsurface damage.
6. SEM micrograph revealed the occurrence of grain pullout, grain fracture and bond fracture of lateral as well as end face of the tool.

Acknowledgment

The authors express their gratitude to "National Institute of Technology", Kurukshetra, India for providing experimental facilities to accomplish this research.

References

[1] R.K. Pal, H. Garg, R.G.V. Sarepaka, V. Karar, Experimental investigation of material removal and surface roughness during optical glass polishing, Mater. Manuf. Process. 31 (2016) 1613–1620, https://doi.org/10.1080/10426914.2015.1103867.

[2] R.P. Singh, S. Singhal, Rotary ultrasonic machining: a review, Mater. Manuf. Process. 31 (2016) 1795–1824, https://doi.org/10.1080/10426914.2016.1140188.
[3] C.C. Tsao, H. Hocheng, Effect of tool wear on delamination in drilling composite materials, Int. J. Mech. Sci. 49 (2007) 983–988, https://doi.org/10.1016/j.ijmecsci.2007.01.001.
[4] Y. Jiao, P. Hu, Z.J. Pei, C. Treadwell, Rotary ultrasonic machining of ceramics: design of experiments, Int. J. Manuf. Technol. Manage. 7 (2005) 192–206, https://doi.org/10.4028/www.scientific.net/MSF.532-533.361.
[5] X. Xiao, K. Zheng, W. Liao, Theoretical model for cutting force in rotary ultrasonic milling of dental zirconia ceramics, Int. J. Adv. Manuf. Technol. (2014) 1263–1277, https://doi.org/10.1007/s00170-014-6216-6.
[6] A.K. Jain, P.M. Pandey, Experimental investigations of ceramic machining using μ-grinding and μ-rotary ultrasonic machining processes: a comparative study, Mater. Manuf. Process. (2016) 1–10, https://doi.org/10.1080/10426914.2016.1198024.
[7] J. Wang, P. Feng, J. Zhang, C. Zhang, Z. Pei, Modeling the dependency of edge chipping size on the material properties and cutting force for rotary ultrasonic drilling of brittle materials, Int. J. Mach. Tools Manuf. 101 (2016) 18–27, https://doi.org/10.1016/j.ijmachtools.2015.10.005.
[8] V. Gupta, P.M. Pandey, An in-vitro study of cutting force and torque during rotary ultrasonic bone drilling, Proc. Inst. Mech. Eng. Part B J. Eng. Manuf. (2016), https://doi.org/10.1177/0954405416673115.
[9] P.K.S.C. Fernando, Z. Pei, M.P. Zhang, X. Song, Rotary ultrasonic drilling of cfrp: effect of process parameters on delamination, in: Proc. ASME 2016 Int. Manuf. Sci. Eng. Conf., 2017: pp. 1–6.
[10] V. Gupta, P.M. Pandey, Experimental investigation and statistical modeling of temperature rise in rotary ultrasonic bone drilling, Med. Eng. Phys. 38 (2016) 1330–1338, https://doi.org/10.1016/j.medengphy.2016.08.012.
[11] A.K. Jain, P.M. Pandey, Study of Peck drilling of borosilicate glass with μ-RUM process for MEMS, J. Manuf. Process. 22 (2016) 134–150, https://doi.org/10.1016/j.jmapro.2016.02.001.
[12] J. Wang, P. Feng, J. Zhang, Reduction of edge chipping in rotary ultrasonic machining by using step drill: a feasibility study, Int. J. Adv. Manuf. Technol. (2016) 1–11, https://doi.org/10.1007/s00170-016-8655-8.
[13] J. Wang, H. Zha, P. Feng, J. Zhang, On the mechanism of edge chipping reduction in rotary ultrasonic drilling: A novel experimental method, Precis. Eng. 44 (2015) 231–235, https://doi.org/10.1016/j.precisioneng.2015.12.008.
[14] Z.H.A. Huiting, Z. Jianfu, An Experimental Study on Rotary Ultrasonic Drilling Small-diameter Holes ofHigh Volume Fraction Silicon Carbide-reinforced Aluminum Matrix Composites (SiCp/Al), Proc. 2017 14th Int. Bhurban Conf. Appl. Sci. Technol. 36 Islam. Pakistan, 10th–14th January, 2017, 2017, pp. 34–39.
[15] F. Ning, H. Wang, W. Cong, P.K.S.C. Fernando, A mechanistic ultrasonic vibration amplitude model during rotary ultrasonic machining of CFRP composites, Ultrasonics 76 (2017) 44–51, https://doi.org/10.1016/j.ultras.2016.12.012.
[16] P. Feng, J. Wang, J. Zhang, J. Zheng, Drilling induced tearing defects in rotary ultrasonic machining of C/SiC composites, Ceram. Int. (2016), https://doi.org/10.1016/j.ceramint.2016.10.010.
[17] N. Cadorin, R. Jitoune, Wear signature on hole defects as a function of cutting tool material for drilling 3D interlock composite, Wear (2015) 742–751, https://doi.org/10.1016/j.wear.2015.01.019.
[18] V. Krishnaraj, R. Jitoune, F. Collombat, Investigations on drilling of multimaterial and analysis by ANN, Key Engg. Mater. 443 (2010) 347–352, https://doi.org/10.4028/www.scientific.net/KEM.443.347.
[19] R. Prakash, V. Krishnaraj, R. Jitoune, J.S. Ahmad, High-speed edge trimming of CFRP and online monitoring of performance of router tools using acoustic emission, Materials (2016), https://doi.org/10.3390/ma9100798.
[20] P. Fernando, M. Zhang, Z. Pei, Rotary Ultrasonic Machining of CFRP: Effects of Abrasive Properties, Proceedings of the ASME (2018), 13th International Manufacturing Science and Engineering Conference.
[21] H. Wang, F. Ning, Y. Hu, Y. Li, Edge trimming of carbon fiber-reinforced plastic composites using rotary ultrasonic machining: effects of tool orientations, Int. J. Adv. Manuf. Technol. 98 (2018) 1641–1653, https://doi.org/10.1007/s00170-018-2355-5.
[22] X. Song, J. Yang, H. Ren, B. Lin, Y. Nakanishi, L. Yin, Ultrasonic assisted high rotational speed diamond machining of dental glass ceramics, Int. J. Adv. Manuf. Technol. 96 (2018) 387–399, https://doi.org/10.1007/s00170-017-1571-8.
[23] A.K. Jain, P.M. Pandey, Experimental studies on tool wear in μ-RUM process, Int. J. Adv. Manuf. Technol. 85 (2016) 2116–2125, https://doi.org/10.1007/s00170-015-8248-y.
[24] J. Wang, J. Zhang, P. Feng, P. Guo, Experimental and theoretical investigation on critical cutting force in rotary ultrasonic drilling of brittle materials and composites, Int. J. Mech. Sci. 135 (2018) 555–564, https://doi.org/10.1016/j.ijmecsci.2017.11.042.
[25] P. Fernando, M. Zhang, W. Cong. Rotary Ultrasonic Machining: Effects of Tool End Angle On Delamination Of CFRP Drilling, Proceedings of the ASME (2017), 12th International Manufacturing Science and Engineering Conference.
[26] A. Goswami, J. Kumar, Optimization in wire-cut EDM of Nimonic-80A using Taguchi's approach and utility concept, Eng. Sci. Technol. Int. J. 17 (2014) 236–246, https://doi.org/10.1016/j.jestch.2014.07.001.
[27] C.P. Mohanty, S.S. Mahapatra, M.R. Singh, An intelligent approach to optimize the EDM process parameters using utility concept and QPSO algorithm, Eng. Sci. Technol. Int. J. 20 (2017) 552–562, https://doi.org/10.1016/j.jestch.2016.07.003.
[28] P. Antil, S. Singh, A. Manna, Electrochemical discharge drilling of SiC reinforced polymer matrix composite using Taguchi's Grey relational analysis, Arab. J. Sci. Eng. (2017), https://doi.org/10.1007/s13369-017-2822-6.
[29] R.S. Walia, H.S. Shan, P. Kumar, Multi-response optimization of CFAAFM process through Taguchi method and utility concept, Mater. Manuf. Process. 21 (2006) 907–914, https://doi.org/10.1080/10426910600837814.
[30] J. Kundu, H. Singh, Friction stir welding of AA5083 aluminium alloy: multi-response optimization using Taguchi-based grey relational analysis, Adv. Mech. Eng. 8 (2016) 1–10, https://doi.org/10.1177/1687814016679277.
[31] N.J. Churi, Z.J. Pei, C. Treadwell, Rotary ultrasonic machining of titanium alloy: effects of machining variables, Mach. Sci. Technol. 10 (2006) 301–321, https://doi.org/10.1080/10910340600902124.
[32] F.D. Ning, W.L. Cong, Z.J. Pei, C. Treadwell, Rotary ultrasonic machining of CFRP: a comparison with grinding, Ultrasonics 66 (2016) 125–132, https://doi.org/10.1016/j.ultras.2015.11.002.
[33] Y. Jiao, P. Hu, Z.J. Pei, C. Treadwell, Rotary ultrasonic machining of ceramics: design of experiments, Int. J. Manuf. Technol. Manage. (2005) 192–206.
[34] Z.C. Li, Y. Jiao, T.W. Deines, Z.J. Pei, C. Treadwell, Rotary ultrasonic machining of ceramic matrix composites: feasibility study and designed experiments, Int. J. Mach. Tools Manuf. 45 (2005) 1402–1411, https://doi.org/10.1016/j.ijmachtools.2005.01.034.
[35] A.S. Bhui, G. Singh, S.S. Sidhu, P.S. Bains, Experimental investigation of optimal ED machining parameters for Ti-6Al-4V biomaterial, FACTA Universisatis Ser, Mech Eng. (2018) 337–345, https://doi.org/10.22190/FUME180824033B.
[36] W.L. Cong, Q. Feng, Z.J. Pei, T.W. Deines, C. Treadwell, Msec 2011–50116 dry machining of carbon fiber reinforced plastic composite by rotary ultrasonic machining: effects of machining variables, Compress. Air. (2011) 1–9, https://doi.org/10.1115/MSEC2011-50116.
[37] M. Komaraiah, P. Narasimha Reddy, Rotary ultrasonic machining—a new cutting process and its performance, Int. J. Prod. Res. (1991) 2177–2187, https://doi.org/10.1080/00207549108948077. 29.
[38] W.L. Cong, Q. Feng, Z.J. Pei, T.W. Deines, C. Treadwell, Rotary ultrasonic machining of carbon fiber-reinforced plastic composites: using cutting fluid vs. cold air as coolant, J. Compos. Mater. (2011), https://doi.org/10.1177/0021998311424625.
[39] C. Zhang, W. Cong, P. Feng, Z. Pei, Rotary ultrasonic machining of optical K9 glass using compressed air as coolant: a feasibility study, Proc. Inst. Mech. Eng. Part B J. Eng. Manuf. 228 (2013) 504–514, https://doi.org/10.1177/0954405413506195.
[40] J. Wang, P. Feng, J. Zhang, W. Cai, H. Shen, Investigations on the critical feed rate guaranteeing the effectiveness of rotary ultrasonic machining, Ultrasonics 74 (2017) 81–88, https://doi.org/10.1016/j.ultras.2016.10.003.
[41] S.Y. Zheng, X.P. Xu, A Comparative Study on Ultrasonic Machining of Red Granite, Solid State Phenom. 175 (2011) 150–156, https://doi.org/10.4028/www.scientific.net/SSP.175.150.
[42] Z.J. Pei, D. Prabhakar, P.M. Ferreira, A mechanistic approach to the prediction of material removal rates in rotary ultrasonic machining, J. Eng. Ind. 64 (1993).
[43] A.K. Dubey, Multi-response optimization of electro-chemical honing using utility-based Taguchi approach, Lect. Notes Mech. Eng. 41 (2009) 749–759, https://doi.org/10.1007/978-81-322-1859-3_21.
[44] P.J. Ross, Taguchi Techniques for Quality Engineering by PHILLIIP J. ROSS 2nd edition McGraw-Hill New-York NY (From F-table at 95% confidence on page number 286).
[45] W. Gu, Z. Yao, H. Li, Investigation of grinding modes in horizontal surface grinding of optical glass, J. Mater. Process. Technol. 211 (10) (2011) 1629–1636, https://doi.org/10.1016/j.jmatprotec.2011.05.006.
[46] N. Churi, Rotary Ultrasonic Machining of Hard-To-Machine Materials, Ph.D. Thesis.